Layer 6 corticothalamic neurons induce high gamma oscillations through cortico-cortical and cortico-thalamo-cortical pathways

S. Russo[1], E. D. Dimwamwa[1], G. B. Stanley[1]

Affiliations:

[1]Wallace H Coulter Department of Biomedical Engineering, Georgia Institute of Technology and Emory University, Atlanta, GA, USA

Abbreviated Title: Corticothalamic induced high gamma oscillations

With 11 text pages, 4 Figures, 1 Supplemental Figure

Correspondence: Garrett B. Stanley
Coulter Department of Biomedical Engineering
Georgia Institute of Technology & Emory University
Atlanta GA 30332-0535
USA
Phone: 404-385-5037
Email: garrett.stanley@bme.gatech.edu

Conflict of Interest. S.R. is the Chief Scientific Officer of Manava Plus. The other authors declare no competing interests.

Funding. This work was supported by NIH National Institute of Neurological Disorders and Stroke BRAIN Grant (NINDS) R01NS104928, NINDS BRAIN Grant RF1NS128896, and National Institute of Biomedical Imaging and Bioengineering (NIBIB) BRAIN Grant R01EB029857.

ABSTRACT

Layer 6 corticothalamic (L6CT) neurons are an excitatory neuron class with projections to both cortex and thalamus. L6CT neurons have been reported to induce multiple effects, including the up- and down-modulation of cortical and thalamic firing rates, and the enhancement of high gamma oscillations in the local field potential (LFP) of the surrounding cortex. These recently reported oscillations offer a neuronal substrate to link recurrent thalamocortical interactions, a critical connection hinging on L6CT neurons, to high frequency oscillations, that have been implicated in several cognitive and pathological conditions. We hypothesize that the high gamma oscillations induced by L6CT neurons in the cortex depend on the dynamic engagement of intracortical and cortico-thalamo-cortical circuits. To test this hypothesis, we optogenetically activated L6CT neurons in NTSR1-cre mice selectively expressing channelrhodopsin-2 in L6CT neurons. Leveraging the vibrissal pathway of awake, head-fixed mice, we presented LED ramp-and-hold inputs of different intensities while recording neuronal activity in the primary somatosensory barrel cortex (S1), the ventral posteromedial nucleus (VPm), and the reticular nucleus (TRN) of thalamus using silicon probes. First, we confirmed that the activation of L6CT neurons induces high-frequency oscillation of S1 local field potential. These oscillations are modulated in frequency, but not in amplitude, across LED intensities and over time. To identify which neuronal classes contribute to these oscillations, we examined the evolution over time of the firing rate of cortical neurons across layers and electrophysiologic cell classes, VPm, and TRN. While the firing rate of most cortical and TRN neurons was steadily suppressed over time, the firing rate of VPm and Layer 4 fast spiking (L4 FS) neurons evolved from being suppressed to being facilitated within 500 ms. Using dimensionality reduction, we found that this pattern reflects two underlying components: one stable component that is represented across all units, and one evolving component that is mainly represented in VPm and in L4 FS neurons, suggestive of differential recruitment of the cortico-cortical vs cortico-thalamo-cortical pathways. Finally, we related the firing rate of each unit to the amplitude and frequency of S1 LFP, finding that the evolution of S1 LFP amplitude weakly correlates with all neurons, while its frequency selectively correlates with VPm firing rate. Taken together, our data suggests that L6CT neurons generate high gamma oscillations in S1 LFP through a combination of intracortical and cortico-thalamo-cortical pathways and can sculpt its oscillation frequency through the cortico-thalamo-cortical pathway. Our findings provide a neuronal substrate for linking recurrent interactions, mediated by L6CT neurons, to the modulations of high gamma oscillations observed in several brain states and pathological conditions.

INTRODUCTION

Layer 6 corticothalamic (L6CT) neurons are an excitatory neuronal class with projections ramified throughout the cortex and spreading to higher and lower order thalamic nuclei. Thanks to these projections[1], L6CT neurons are strategically positioned for modulating the thalamocortical network[2–4] and conveying top-down modulatory feedback. It is not surprising that neurons implicated in such functions, and potentially representing a pivot in corticothalamic communication, have been investigated to illuminate their electrophysiological and behavioral functions in the thalamocortical network. To understand how L6CT neurons affect the brain network and thus contribute to behavioral and cognitive functions, their effects were investigated from two main perspectives: their impact on other neurons, and their impact on the population-level oscillations.

While multiple previous studies investigated how L6CT neurons affect the firing rate of other neurons, there are only a few reports about their effects at the local field potential (LFP) level. L6CT neurons have been reported to induce high gamma oscillations in the local field potential of S1. The spectral analysis of L6CT-induced oscillations revealed that their frequency peaks between 60 to 250 Hz, falling in the rage of activity referred to as high-gamma oscillations or the "ripples" band[5,6]. Importantly, the interruption of L6CT activation immediately abolishes high gamma oscillations that are replaced by slow oscillations peaking approximately at 5 Hz. The phase of these oscillations is locked to the spikes of L6CT and VPm neurons, thus suggesting a relationship between these oscillations and the activity of L6CT and VPm neurons *in vitro* and in the auditory pathway[7,8]. This observation suggests that the oscillations induced by L6CT neurons may be mediated by both intracortical circuits, through L6CT neurons, as well as cortico-thalamo-cortical circuits, through VPm neurons. Yet, the extent to which these two circuits contribute to the emergence of high-gamma oscillations is still elusive and expands the long-lasting question of whether their effect is mainly mediated by intracortical or cortico-thalamo-cortical projections[9].

Given the central role of L6CT neurons in corticothalamic communication, the idea that they provoke fast oscillations aligns with works implicating high gamma oscillations in thalamocortical communication[10], as these oscillations can be generated by subcortical structures[11] and in particular by thalamocortical axons[12]. High gamma oscillations can be generated by the activation of multiple cortical and subcortical neurons, including Layer 2/3 pyramidal neurons[13], parvalbumin neurons in the cortex[14,15] and in the basal forebrain[16], excitatory cortical neurons[17], and hippocampal neurons[18]. This growing effort to illuminate the origins of high gamma oscillations stems from their implication in several cognitive functions, such as attention[19], memory processing[20,21], coordination across areas[22], and cognitive tasks[23]. In support of the critical role of gamma oscillations, the disruption of gamma activity has been associated with several disorders, such as Alzheimer's Disease, fragile X syndrome, and schizophrenia[24–26]. Illuminating how distinct neuronal populations contribute to high gamma oscillations would broaden our understanding of the neuronal bases of cognition and behavior, potentially offering new therapeutic targets for several neurologic and psychiatric conditions.

Given the above, the ability of L6CT neurons to generate high gamma oscillations in several areas raises several questions: do L6CT neurons originate high gamma oscillations also in other areas in awake mice? How are these oscillations shaped and modulated? How do they relate to

neuronal activity? Here we hypothesize that L6CT neurons drive high gamma LFP oscillations in the S1 of awake mouse, and that these oscillations are cooperatively mediated by intracortical and thalamocortical pathways. We tested this hypothesis by manipulating the activity of L6CT neurons through targeted optogenetic manipulations and examining their effects on the LFP, cortical, and thalamic neurons. Our results indicate that the optogenetic activation of L6CT neurons induces high gamma oscillations in the somatosensory pathway of awake mice; while the amplitude of these oscillations is stable, their frequency is determined by light intensity and varies over time. To identify the neuronal circuits regulating this activity, we examined the firing rates of cortical and thalamic units, finding a similar evolution in VPm and layer 4 fast spiking (L4 FS) neurons, that, interestingly, share a common underlying dynamic. Finally, we found that the evolution of VPm firing rate over time covaries with the frequency of S1 high gamma oscillations, thus confirming that VPm holds a critical role in sculpting the frequency of S1 LFP oscillations.

RESULTS

To investigate how L6CT neurons affect the LFP activity in S1, we activated L6CT neurons through targeted optogenetic manipulation while simultaneously recording extracellular electrophysiological activity across layers in S1 with silicon probes in awake mice. Specifically, we injected NTSR1-Cre mice with a recombinant adeno-associated virus (rAAV) encoding eYFP fused with Cre-dependent Channelrhodopsin2 (ChR2) in S1 (Figure 1A). To drive spiking activity in L6CT neurons, we administered blue light through a 400 um fiber conducting light from a 470 nm LED driven with a ramp-and-hold waveform (ramp: 250ms, hold: 500ms, hold at 16 mW/mm^2) positioned on the skull above S1 (Figure 1B). This optogenetic activation of L6CT neurons drove high frequency activity in the LFP of S1, shown across cortical depths before and during LED stimulation (Figure 1C). Qualitatively, this high frequency activity started briefly after the light onset and persisted as long as the light was on, although the high frequency pattern varied over time. Specifically, the light onset drove fast activity, that progressively slowed over time. We computed the power spectral density (PSD) of the LFP signal induced in the 250 to 750 ms window during L6CT activation and in periods of time with no L6CT activation of equivalent duration, finding a striking difference in the power of high frequency activity, consisting of a large narrow-band peak at approximately 150 Hz induced by the L6CT activation (Figure 1D, top). This effect was highly reproducible across recordings, but whose peak frequency changed from 80 to 180 Hz depending on the subject and light intensity, as illustrated in the colormap of spectral power over this frequency band in Figure 1D (bottom).

To characterize the properties of the L6CT-induced high gamma oscillation, we high-pass filtered the signal above 65 Hz to remove line-noise and optoelectric artifacts, and separated for each time bin its amplitude, quantified as the absolute value of the voltage, from its frequency, quantified as the frequency with the maximum power in the time-frequency decomposition (Figure 2A). Inspection of the amplitude and time-frequency dynamics across all light intensities revealed that the oscillation amplitude rapidly increased and decreased during the light ramp (0-250 ms) and then remained stable during the hold period (250-750 ms) of the light. Instead, the oscillation frequency progressively increased throughout the light ramp and then progressively declined during the hold period. The time-course of the oscillation amplitude and frequency averaged across subjects confirmed this pattern: the oscillation amplitude peaked early during the ramp phase and, after a brief reduction, remained stable

over time; conversely, the oscillation frequency peaked at approximately 200 ms and then steadily decreased over time. Importantly, these observations confirm that the ramp phase exhibits transient effects of the stimulation that disappear during the hold phase. Interestingly, these traces suggested that distinct light intensities led to distinct LFP oscillations (Figure 2B). To investigate the difference in the oscillations induced by distinct light intensities, we averaged over time (250-750 ms) for each light intensity the oscillation amplitude and frequency and compared them across light intensities (Figure 2C). We found that while the oscillation amplitude was invariant across light intensities (Analysis of Variance – ANOVA repeated measures; $p=0.07$; Amplitude at 8 mW/mm^2 : 2.6 μV; Amplitude at 30 mW/mm^2 : 2.8 μV),the oscillation frequency significantly increased with higher light intensities (ANOVA repeated measures; $p<0.001$; Frequency at 8 mW/mm^2: 104 Hz; Frequency at 30 mW/mm^2 : 130 Hz). Next, we examined the evolution of the oscillation over time in the hold period. To this aim, for each light intensity level and time window (early: 250-500 ms; and late: 500-750 ms, accounted for the relative Hamming windows; see methods), we averaged over time the oscillation amplitude and frequency (Figure 2D). We found that the oscillation amplitude was marginally modulated over time (Wilcoxon signed-rank test; $p<0.01$ in 8 mW/mm^2 and 16 mW/mm^2; Average amplitude at 30 mW/mm^2: Early=2.85 μV; Late=2.82 μV), while the oscillation frequency consistently decreased from the early to the late time window (Wilcoxon signed-rank test; all $p<0.001$; Average frequency at 30 mW/mm^2: Early=122 Hz; Late=136 Hz).

Changes in the LFP oscillation frequency are associated with changes in the overall excitability of the circuit[27], that is known to be associated with different firing rates across distinct cell classes in the cortex[28]. Accordingly, we hypothesized that this evolution of excitability as inferred by changes in the LFP oscillation frequency would reflect in distinct modulation in the firing rates of distinct cell classes. L6CT neurons have two main projection targets: cortical (both excitatory and inhibitory neurons, even though with different strengths, in deep layers)[3] and thalamic neurons (including the reticular [TRN] and ventroposteromedial nucleus of the thalamus [VPm])[4,9]. To investigate the impact of the changes in excitability reflected in the LFP on different cell classes in cortex and in sub-cortical recipients of L6CT projections, we examined the spiking activity induced by the ramp-and-hold activation of L6CT neurons across cortical layers and electrophysiologic cell classes in the cortex (Regular Spiking [RS] and Fast spiking [FS]), VPm, and TRN. We found that cortical and VPm units were initially suppressed by L6CT activation, while TRN units were enhanced across all light intensities, as shown in our previous study in this same dataset[29] (Figure 3A). The suppression of most cortical neurons persisted throughout the L6CT activation with minimal reduction in most cortical neurons across all light intensities, with the exception of Layer 4 FS neurons in which, at higher light intensities, the initial suppression was followed by a remarkable increase in firing rate, to the point of becoming facilitated at the end of the light modulation with respect to their baseline. Another exception were L5 FS neurons, that were suppressed by the hold phase of the light stimulus at lower light intensities and almost not modulated at intermediate light intensities. Interestingly, VPm neurons exhibited a similar pattern to L4 FS neurons, and TRN neurons were facilitated during the light activation. To characterize this evolution of the firing rate over time, we compared the average firing rate of the early (250-500 ms) and late (500-750 ms; Figure 3B) windows of the constant light stimulation. We found a small but significant increase in the firing rates of most neuronal classes except for L6CT and L6 FS units. This increase was particularly remarkable in VPm and L4 FS neurons at higher light intensities (Increase at 8 mW/mm^2: VPm=0.4 Hz; L4 FS=0.6 Hz; Increase at 30 mW/mm^2: VPm=2.1 Hz; L4 FS=3.4

Hz). Contrary to most other neurons, TRN neurons were initially facilitated by L6CT activation, and this facilitation reduced over time across all light intensities (Reduction at 30 mW/mm^2: 1.9 Hz). Interestingly, this effect was larger at higher light intensities.

Since L4 neurons are the main target of VPm neurons, it is possible that similarities in their firing rate patterns may reflect shared underlying dynamics. To capture these underlying dynamics, we applied Principal Component Analysis to the average time course of the firing rates of each class of neurons (PCA; Figure 3C), finding that two components were sufficient to capture ~99% of the variance across firing rates (see scree plot in Figure S1). Both components were characterized by a rapid onset in the first tens of milliseconds from the beginning of the ramp, but the first component was stable over time, as indicated by the constant weight throughout the early and late window, while the second component increased over time, as indicated by the inversion of the weights' polarity from the early to the late window. These two patterns are reminiscent of the stable time course of most cortical neurons and of the rapidly shifting time course of VPm and L4 FS units, respectively. This was confirmed by the inspection of the weights of each component across the different cell-type classes, showing that the stable component was represented across all cortical layers, VPm and TRN, while the shifting component was selectively represented with positive weights in VPm and L4 FS units at higher light intensities. Interestingly, the stable component exhibited positive weights in L6CT and TRN neurons, and negative weights in all other neurons.

The LFP analysis indicated that L6CT activation induced an oscillation in the high gamma range whose amplitude was stable over time, while its frequency shifted during the constant light window. The analysis of single-unit firing rates indicated that most cortical units exhibited a stable modulation of their firing rates over time, while the firing rates of VPm and L4 FS units shifted from suppression to facilitation. The observation of similar LFP and single-unit dynamics, both consisting of an element stable over time and an element shifting in the timescale of 500 ms, suggested a potential relationship between them. To investigate the relation between LFP and spiking dynamics, we correlated the firing rate of each neuron with the simultaneously recorded LFP oscillation amplitude and frequency (Spearman's correlation). For each class of neurons, we assessed the strength of the correlation by computing the percentage of neurons showing a significant correlation ($p<0.05$) with the LFP amplitude and the average Spearman's Rho across neurons showing a significant correlation (Figure 4A). First, this analysis revealed that L6CT activation increases the percentage of significant correlations between the firing rate of neurons from any class and the LFP amplitude. Additionally, we found that while most neurons in each neuronal class were significantly correlated with LFP amplitude during L6CT activation, the correlation strengths were close to 0 across all light intensities, suggesting a negligible relationship between the LFP amplitude and all cell class firing rates (max: 0.12; min: -0.1; Figure 4A).

We next correlated the LFP frequency with the single-unit firing rate of all cell classes in a similar manner. In contrast to the relationship with LFP amplitude, the firing rates of most cortical neurons across all classes including L4 Fs neurons were not significantly correlated with LFP frequency, except for L2/3 FS neurons at low light intensity. Another exception was the VPm neurons, as most of them were significantly and negatively correlated with LFP frequency, and with remarkable correlation strengths across all light intensities (Figure 4B). Interestingly, while a relatively small number of L6CT neurons were significantly correlated with LFP frequency, they were the only class of neurons showing a positive correlation with the LFP frequency.

DISCUSSION

In this study, we show that L6CT neurons induce high gamma oscillations in S1[7,8], where the frequency of these oscillations, but not their amplitude, is a function of the level of activation of L6CT neurons and varies over time. In response to L6CT activation, the firing rate of several cell classes exhibited an evolution in activity characterized by an initial suppression that gradually decreases, with VPm and L4 FS neurons exhibiting a remarkable switch from being suppressed to being facilitated. These spiking activity profiles were captured by two underlying components, one of which is stable over time and is represented in all neurons, and the other of which is shifting over time and is represented primarily in VPm and L4 FS neurons. By relating the spiking activity profiles of each neuronal class to LFP oscillations, we found that the firing rate of all neuronal classes was only weakly correlated with LFP amplitude, while LFP oscillation frequency was selectively and strongly correlated with VPm neuron activity.

Interestingly, we found that LFP oscillation frequency, but not amplitude, depends on L6CT activation intensity. This fine and selective modulation of the LFP frequency complements the role of parvalbumin inhibitory neurons, that have been shown to modulate LFP gamma oscillation amplitude but not frequency[14]. The finding that L6CT neurons can finely sculpt the frequency of high gamma oscillations suggests that they may hold a critical role in situations in which the oscillation frequency undergoes narrow-band frequency modulations, such as attention[30], seizures[31–33], dyskinesia[34], and perception[35].

One important observation here is that the temporal profile of LFP oscillation frequency correlated with VPm firing rate. This suggests that VPm may hold a key role in mediating the modulation of S1 LFP frequency over time. This finding aligns well with previous studies showing that the thalamus can shape the narrow-band high gamma oscillation frequency in cortical areas[36] and that high gamma oscillations reflect thalamocortical communication[10].

Our observation that at low light intensities L6CT neurons suppress downstream VPm neurons agrees with previous reports of L6CT-induced suppression of thalamic neurons in the visual thalamus and *in vitro* in S1[7,37]. This may be explained by L6CT spikes recruiting strong inhibitory TRN inputs to VPm that dominates L6CT's direct excitatory inputs to VPm[29,38]. Interestingly, L6CT spikes induce a prolonged suppression of VPm at the low light intensities tested here, clearly different from the hyperpolarization that disinhibits T-type calcium channels mediating the pause-and-burst pattern observed after optogenetic VPm inhibition[39] and TRN excitation[40,41] that has been associated with slower LFP rhythms. One potential explanation for this difference is that L6CT neurons simultaneously depolarize and hyperpolarize VPm, through their excitatory terminals or through TRN-mediated inhibition, respectively. Previous simulations suggest that the coexistence of TRN hyperpolarizing inputs and cortical depolarizing inputs may keep thalamocortical neurons in a slightly hyperpolarized state that is below spiking threshold, but above the threshold required to disinhibit T-currents and, thus, evoke bursts[40]. As a result, L6CT spikes may be able to keep thalamocortical neurons in a "sweet spot" of suppression, in which reduced spiking activity can be maintained over prolonged windows of time and gradually increase, instead of abruptly switching to a bursting regime.

The finding that L6CT spikes suppress, at least at low light intensities, most cortical layers naturally raises a question about what mechanisms underly the emergence of the cortical suppression induced by L6CT activation. Indeed, there are two mechanisms that may contribute to cortical suppression, and that may coexist. The first mechanism is disynaptic

inhibition through cortical inhibitory interneurons. Previous studies have suggested that the intracortical projections of L6CT neurons in the primary visual cortex strongly recruit local inhibitory neurons which suppresses the cortex[4,37]. Along this line, previous analyses on this same dataset indicate that L6CT activation increases the firing rate of a subset of FS neurons in S1 L4-6. An alternative mechanism is the withdrawal of excitatory inputs due to suppression of VPm. Indeed, thalamic inputs are key to sustain cortical activity, and their suppression greatly reduces or even abolishes cortical firing[40,42]. In support of this mechanism, our results show that one single factor captures the shift of firing activity in both VPm and L4 FS neurons, a primary target of VPm neurons. Hence, we suggest that the withdrawal of excitatory inputs from VPm contributes to the L6CT-induced suppression, at least in L4 FS neurons. By contrast, the other cortical neurons mainly present stable suppression, advocating for intracortical suppression. Overall, our analyses suggest that intracortical inhibition contributes to the suppression of cortical activity across different layers throughout the entire window, while the withdrawal of excitatory VPm inputs contributes to it only for a relatively short time at the beginning of L6CT activation.

The firing rate dynamics induced by L6CT activation can be exhaustively recapitulated by two principal components, with one stable component represented across all neurons and one component that shifts over time represented only in VPm and L4 FS neurons. These two different progressions over time suggest two distinct trajectories that may reflect the short-term plasticity patterns typical of intracortical and thalamic L6CT synaptic terminals, respectively. Indeed, it has been previously reported that, within 1 second, the excitatory synaptic currents induced by the activation of L6CT neurons in their intracortical terminals varied from a ~60% increase to a ~20% decrease, depending on the targeted layer[3]. In response to similar activation inputs, L6CT terminals in VPm showed strikingly larger effects, with a ~400% increase of fast glutamatergic currents and a drop of ~70% in the disynaptic GABA hyperpolarizing currents[7,43]. While the stable component resonates with the relatively weak depression of intracortical circuits[3], the shifting component observed in VPm and L4 FS neurons resonates with the strong facilitation of excitatory synapses and suppression of inhibitory synapses described in the thalamus[7]. Indeed, our findings align with previous reports that L6CT activation switches, in the timescale of one second, from suppressing to facilitating VPm neurons[7]. Overall, the two factors that we isolated may recapitulate the downstream consequences of synaptic adaptation of L6CT intracortical and thalamic projections, respectively.

Interestingly, the rapidly shifting component described here is selectively expressed at the cortical level in L4 FS neurons. While the specific regain of activity in L4 activity following the initial suppression may be explained by the strong thalamocortical projections from VPm to L4, the selective increase of firing in L4 FS, but not RS, neurons cannot be explained by structural connectivity alone[3,44,45]. Instead, the selective shift in firing rate of L4 FS units may be explained by their membrane properties: PV+ neurons, the transcriptomic class associated to fast spiking activity, can spike in response to one single excitatory input, while excitatory neurons require multiple synchronous excitatory inputs in order to spike[46]. As a result, the gradual regain of VPm spikes is likely to drive FS neurons more easily than RS neurons.

L6CT neurons have been implicated in many functions and behaviours[1,47,48], as they are a strategic junction between cortex and thalamus, capable of modulating both intracortical and thalamocortical loops. Furthermore, the ability of L6CT neurons to induce time- and intensity-dependent oscillations in the cortex, associated with both facilitatory and suppressive effects

on downstream neurons as well as synchrony-dependent changes across cortex and thalamus[29], corroborates the idea that L6CT neurons can flexibly adapt to exert a myriad of functions. Multiple studies have suggested that L6CT neurons may be implicated in higher cognitive functions, and this idea is further supported by our finding that they can sculpt the frequency of high gamma oscillations, which have been widely implicated in higher cognitive functions[19,23,49].

While our findings demonstrate that L6CT neurons have the capacity to modulate the firing rate of downstream units and LFP frequency, they leave an open question as to the extent to which they serve this role in natural conditions. Indeed, the role of L6CT neurons in natural conditions, such as in modulating attention levels and shaping behaviours, is still elusive. Further investigation is needed to clarify the role of L6CT neurons in their physiological range of activity. Similarly, we explored the effects of L6CT activation on the evolution of S1 LFP spontaneous activity over time, which raises the question of whether responses to sensory stimuli are differentially modulated over different L6CT activation time windows. Finally, while our study leverages correlational analyses to establish a link between VPm firing rate and LFP oscillation frequency, verifying a causal link between them will require future causal experiments.

METHODS

Data acquisition

In this paper we leverage the dataset published in Dimwamwa et al[29]. This dataset consists of the optogenetic stimulation of S1 in 12 NTSR1-cre (B6.FVB(Cg)-Tg(Ntsr1-cre)GN220Gsat/Mmcd, MMRRC) adult mice aged between 6 weeks and 6 months. In brief, mice were kept in a reversed light-dark cycle at 65-75°F and 40-60% humility. Mice underwent a first surgical procedure, thinning the skull above S1 (as identified by stereotactic coordinates), intrinsic imaging during whisker stimulation to map the location of the barrels associated with each whisker, were injected in the primary somatosensory cortex (S1) with 800 mL of cre-dependent AAV5-EF1a-DIO-hChR2(H134R)-eYFP.WPRE.hGH[1,50] (UPenn Vector Core), and were habituated to the experimental rig. After at least 3 weeks from the injection, mice were anesthetized (induction: isoflurane 5%; Maintenance: isoflurane 0.5-2%) to open 2 burr holes above VPm (as identified by stereotactic coordinates) and S1 (as identified by intrinsic imaging).

The day of the experiment, mice were head fixed on the experimental rig and the electrodes were inserted in S1 (A1x32-5 mm-25-177-A32, A1x32-Poly3-5mm-25s-177-A32, A1x64-Poly2-6mm-23s-160, or A1x64-Edge-6mm-20-177-A64, Neuronexus, Ann Arbor, MI), VPm (A1x32-Poly3-5mm-25s-177-A32, Neuronexus, Ann Arbor, MI), and TRN (Buzsaki32 or A1x32-Poly3-5mm-25s-177-A32, Neuronexus, Ann Arbor, MI). Electrophysiological data were acquired through a Cerebrus acquisition system (Blackrock neurotech, Salt Lake City, Utah) or TDT RZ2 Bioamp Processor (Tucker Davis Technologies, Alachua, FL) with a sampling frequency of either 30,000 or 24,414.0625 Hz.

An optical fiber (400 nm diameter) was connected to a blue LED source (470 nm wavelength) and positioned to shine light above the craniotomy in S1. L6CT neurons were activated using ramps-and-hold light waveforms (ramp: 250 ms; hold: 500 msec; light intensities: 8, 16, 24, and 30 mW/mm^2). Additionally, to determine sensory responsiveness, mice underwent whisker stimulation through a galvanometer deflected with a sawtooth waveform at a velocity of 300 deg/s in the caudo-rostral direction. Whisker stimuli were administered with 10 Hz frequency in blocks of 1 second. Videography was acquired under infrared illumination using CCD cameras triggered at 30 or 200 Hz. The LED source, the galvanometer, and the camera were controlled through custom scripts in MATLAB and Simulink Real-Time (MathWorks, Natik, MA) at 1 kHz. For a detailed description of the experimental procedures see Dimwamwa et al[29].

Videography processing

Videography data were analyzed using FaceMap[51]. The analysis was restricted to the region of the video with the mouse whiskers, and that region was used to compute the motion energy[52,53]. The motion energy was then smothered over time and all trials with motion energy above a fixed threshold, indicating whisker movements, were excluded, and all subsequent analyses were performed on the remaining trials[29].

Single-unit data preprocessing

Recorded data were high pass filtered (500 Hz cutoff frequency; 3rd order Butterworth filter), median filtered across channels, sorted using Kilosort[54], and manually curated using Phy2[55]. We considered only units with signal-to-noise ratio>3 and less than 2% of the spikes violating a 2ms refractory period. S1, VPm, and TRN units used for analyses were required to be

sensory responsive[29,53]. S1 neurons were classified as regular-spiking or fast-spiking based on the mean spike waveform[56] and each neuron was assigned to a layer relative to the center of layer 4 (as identified by current source density analysis)[57,58]. L6CT neurons were identified using the stimulus-associated spike-latency test (SALT)[59]. Using the 10Hz train of sawtooth whisker stimuli of 1 second, VPm neurons were further identified by a latency <15 ms for the first stimulus and <20 ms for the last stimulus. Furthermore, VPm neurons were required to have a waveform width >0.3 ms.

Single-unit data processing

We computed peri-stimulus time histograms (PSTHs) from -750 to 750 ms around the onset of the ramp-and-hold light with bins of 1.5 ms. PSTH were smoothed by applying a moving average (15 ms smoothing window, movmean function from matlab).

The mean firing rate of each neuron during the early (250-500) and late (500-750) window was computed by averaging the firing rate in the respective window.

To perform the dimensionality reduction analysis, the average PSTH for each cell type was cut from -100 to +750 ms around the light onset and the average PSTH of the baseline was subtracted from the entire PSTH. Dimensionality reduction was performed using principal component analysis (PCA; pca function from Matlab). To explain 99% variance, we selected two components (see scree plot in Figure S1) and reported the weights and time course of each component.

LFP data processing

LFP data were downsampled to 1000 Hz (lowpass filter 200 Hz), highpass filtered (65 Hz cutoff frequency; 3rd order Butterworth filter,) and segmented from -750 to 750 ms around the onset of ramp-and-hold light manipulations.

To obtain the time course of the absolute voltage for each channel, we rectified the voltage and averaged it across trials. To obtain the oscillation peak frequency of each channel, we decomposed the voltage of each channel in the time-frequency domains (newtimef function from eeglab[60]) and identified, for each time bin and channel, the frequency showing the maximum power.

We quantified the absolute amplitude and the average peak frequency of each channel in the early and late window by averaging the absolute amplitude and the oscillation frequency, respectively, for each window. For these quantifications, we accounted for the hamming windows of the filtered data by reducing the early and late windows to 245-500 ms and 500-745 ms for the absolute voltage and 292-500 ms and 500-708 ms for the oscillation frequency.

Statistical comparisons

The statistical analyses comparing the LFP amplitude and frequency across different light intensities were performed using a repeated measures ANOVA test.

Statistical analyses comparing early and late window in units firing rate, LFP amplitude, and LFP frequency between, were performed using Wilcoxon signed-rank tests.

The correlations between single unit PSTH and LFP amplitude and frequency were computed as follows: PSTHs were resampled to the same frequencies of LFP amplitude and frequency; signals were cut in the stable light window (250-750 ms) and correlated over time with the simultaneously recorded LFP amplitude and frequency (Spearman's correlation).

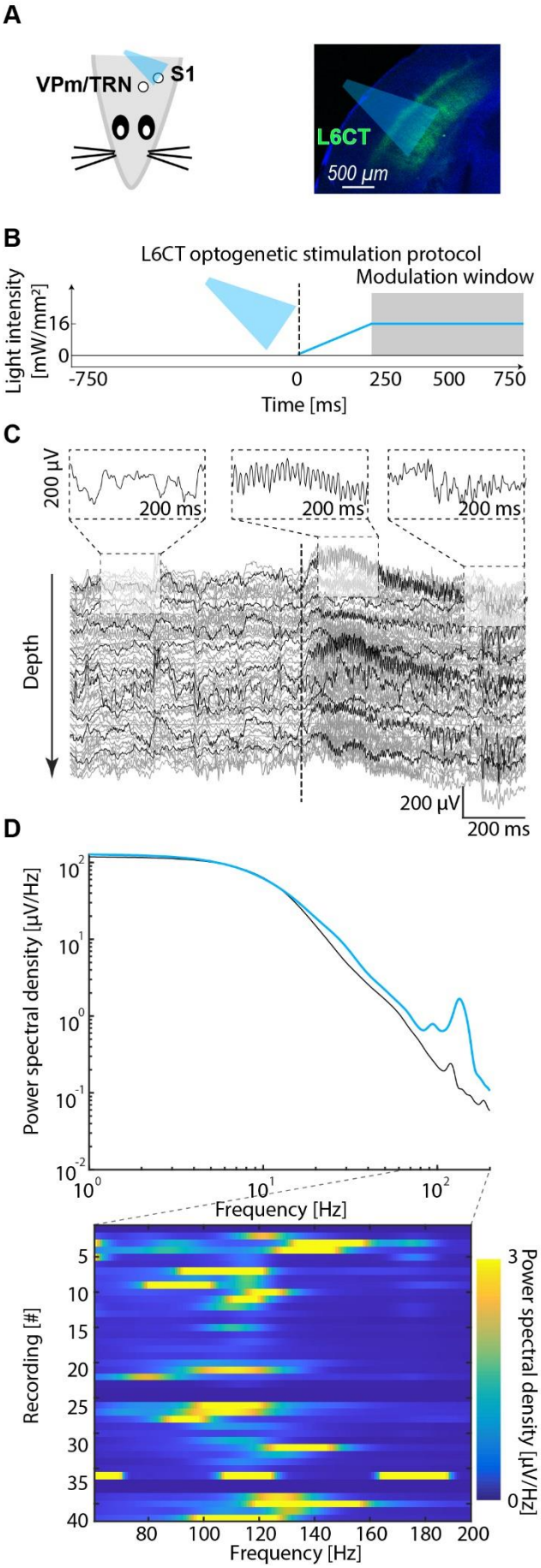
A
VPm/TRN
S1
L6CT
500 µm
B
L6CT optogenetic stimulation protocol
Modulation window
Light intensity [mW/mm²]
16
0
-750
0
250
500
750
Time [ms]
C
200 µV
200 ms
200 ms
200 ms
Depth
200 µV
200 ms
D
Power spectral density [µV/Hz]
Frequency [Hz]
Recording [#]
5
10
15
20
25
30
35
40
80
100
120
140
160
180
200
Frequency [Hz]
3
0
Power spectral density [µV/Hz]

Figure 1. Optogenetic activation of L6CT neurons induces high gamma oscillations in the local field potential of S1. A. The left panel shows the schematic setup for the insertion of silicon probes in S1 and VPm during optogenetic activation of L6CT neurons. The right panel shows in blue the S1 histological section with DAPI staining and in green L6CT neurons marked with the eYFP fluorophore. **B.** The light was administered through a ramp-and-hold waveform to minimize transient effects of light. **C.** Representative traces recorded from all the silicon probe channels in S1 in one trial showing that the optogenetic activation of L6CT neurons induces high-gamma activity in the broadband local field potential (LFP). At the time of the onset of the stimulus, the LFP shows a slow deflection superimposed to high frequency oscillations. In black a subset of traces was highlighted for ease of visualization. The insets show how the oscillation changes from baseline to the beginning and end of the L6CT activation. **D.** Top: Representative broadband power spectral density (PSD) of the activity induced by the optogenetic activation of L6CT neurons during the hold-phase (light blue trace) and without optogenetic stimulation (black trace). The PSD shows that L6CT optogenetic activation generates narrowband LFP oscillations in the high gamma range. Bottom: PSD of the activity induced by L6CT activation in each recording in the 65-200 Hz band.

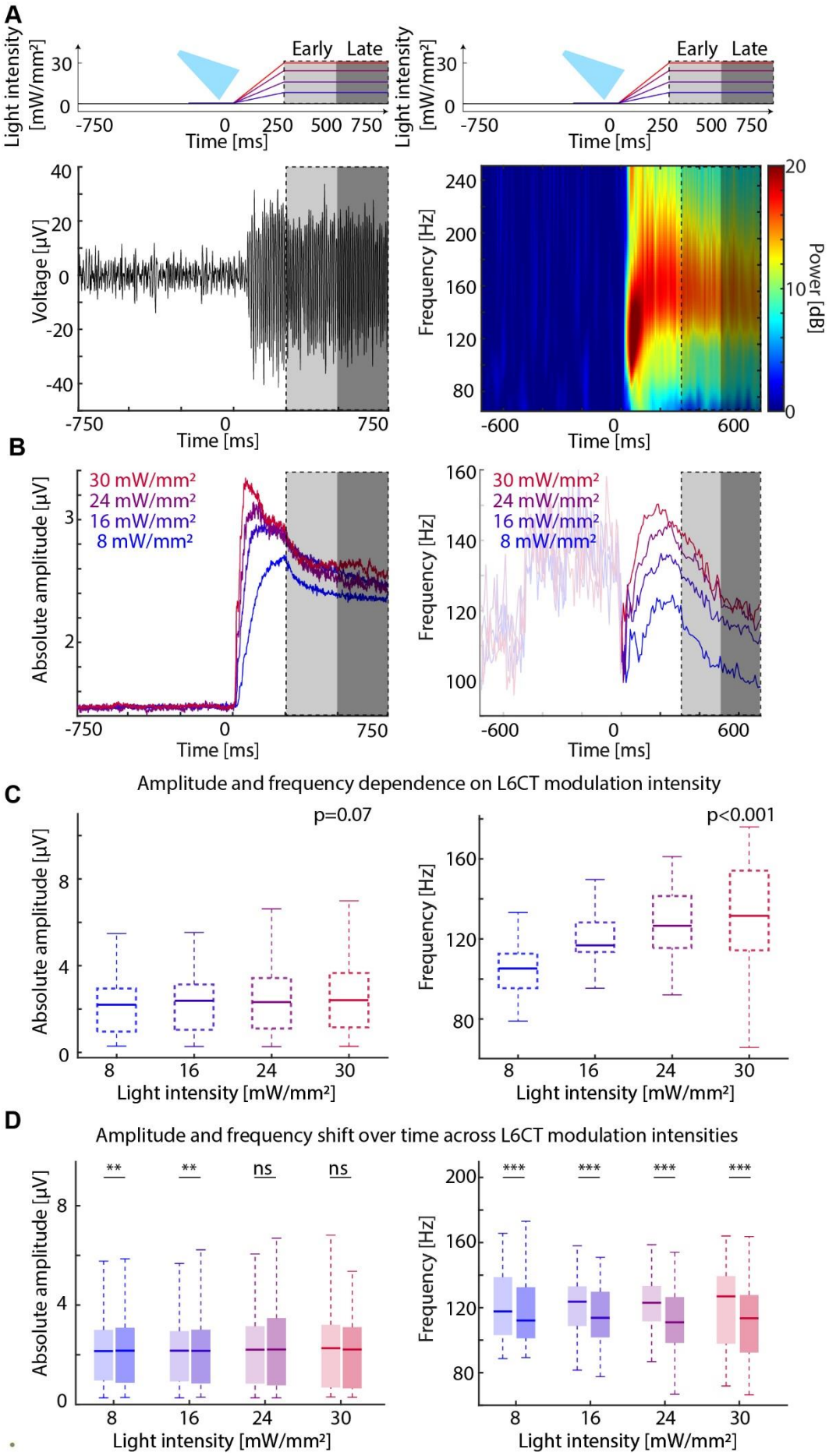
A
Light intensity [mW/mm²]
Early
Late
Time [ms]
Voltage [µV]
Frequency [Hz]
Power [dB]
B
30 mW/mm²
24 mW/mm²
16 mW/mm²
8 mW/mm²
Absolute amplitude [µV]
Frequency [Hz]
Time [ms]
C
Amplitude and frequency dependence on L6CT modulation intensity
p=0.07
p<0.001
Absolute amplitude [µV]
Frequency [Hz]
Light intensity [mW/mm²]
D
Amplitude and frequency shift over time across L6CT modulation intensities
**
ns
***
Absolute amplitude [µV]
Frequency [Hz]
Light intensity [mW/mm²]

Figure 2 – The high gamma LFP oscillations induced by L6CT neurons are intensity- and time-dependent. A. The top panels show that the optogenetic activation of L6CT neurons was administered through ramp-and-hold waveforms of 4 different light intensities (color coded by light intensity). The area outlined by the dashed line highlights the time window during the hold-phase of the light waveform. The shaded areas in light and dark grey highlight the early and late windows of the hold-phase of the light waveform, respectively. The bottom panels show one representative S1 LFP (left) and time-frequency decomposition (right) of the oscillation induced by the optogenetic activation of L6CT neurons showing the emergence of high gamma oscillations. The shaded regions in the bottom panel highlight smaller windows with respect to the top panels to account for the Hamming window of the filtering. **B.** The traces show the absolute voltage (left) and frequency (right; baseline window shaded) of the LFP over time across different light intensities and averaged across subjects (color code as in panel A). **C.** The boxplots show the distribution of the absolute voltage (left) and frequency (right) of the LFP during the hold-phase across different light intensities (line: median; box: 25 and 75 percentiles; whiskers: minimum and maximum value; color code as in panel A; ANOVA repeated measures). **D.** The boxplots show the distribution of the absolute amplitude (left) and frequency (right) across L6CT activation intensities between early (lighter) and late window (darker; color code as in panel A; Wilcoxon signed-rank tests).

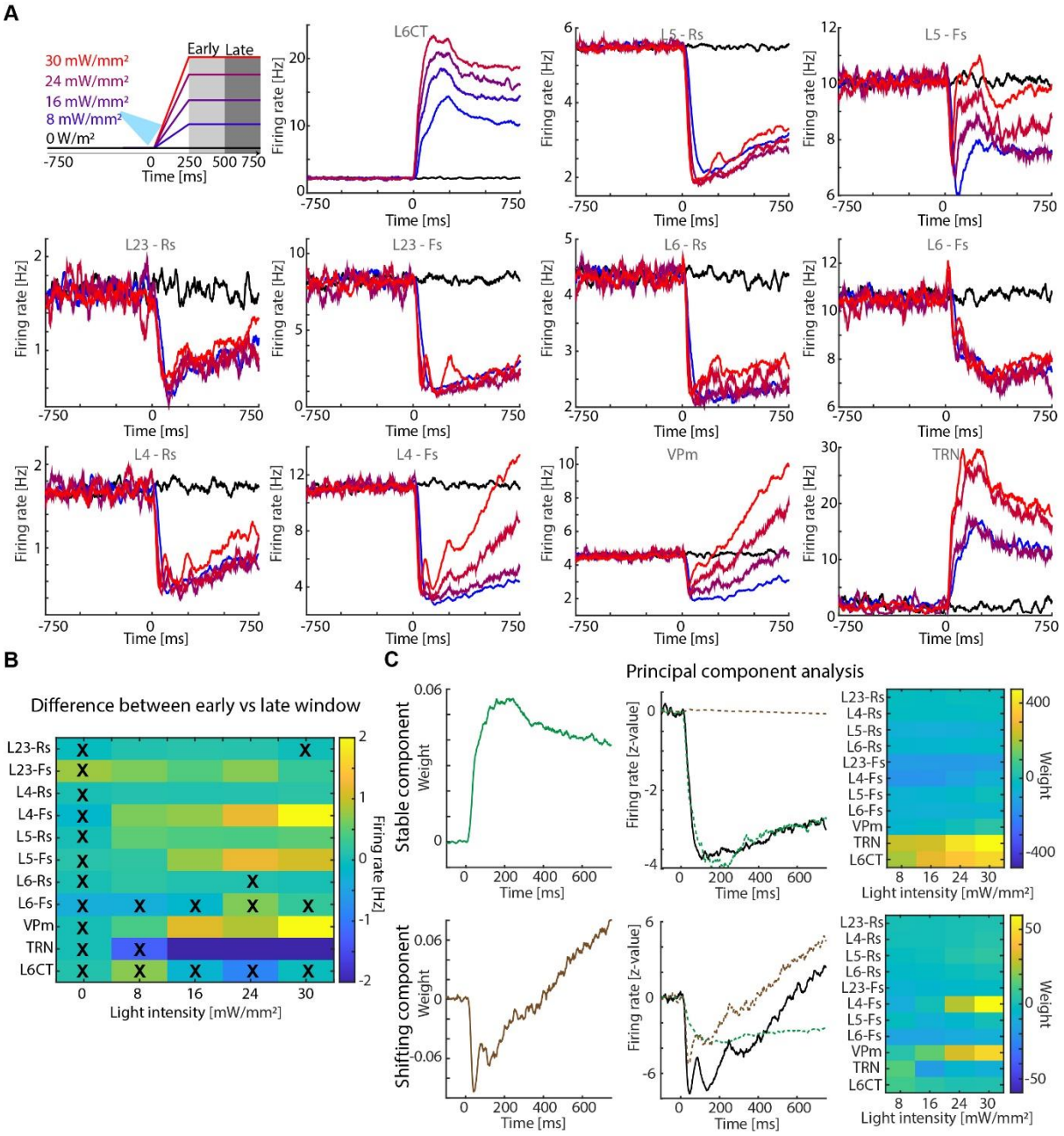

Figure 3 – L6CT activation induces two distinct firing profiles across regions, layers, and neuronal classes. A. The top left panel shows the ramp-and-hold light manipulation protocol showing the time windows classified as early (light grey) and late (dark grey). The other panels show the average firing rate over time induced by ramp-and-hold optogenetic stimulation of L6CT neurons across multiple layers and classes of neurons. **B.** Comparison between the early and late firing rates across layers and neuronal classes (Wilcoxon signed-rank test; "x" indicates non-significant p>0.05). **C.** The left panels show that PCA summarizes the effect of L6CT neurons on other neurons in two components, one stable (green, top panels) and one shifting over time (brown, bottom panels), explaining ~99% of the variance. The central panels illustrate the back projection of the components on two representative firing rate traces (L23 FS and L4 FS, respectively), showing how firing rates in different neuronal classes can either reflect only the stable component or a sum of both components. The right panels show that the stable component is represented across all cortical neuronal classes,

VPm, and TRN, while the shifting component is mainly represented in VPm and L4 FS neurons.

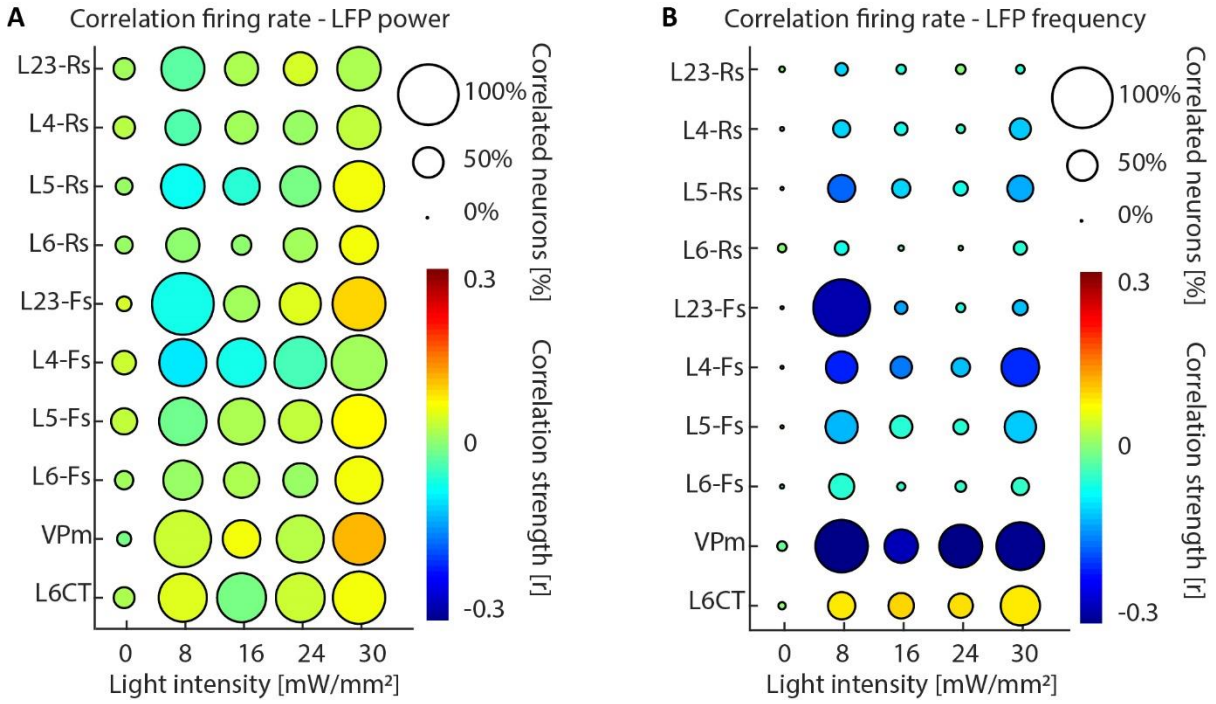

Figure 4 – Relation between high-gamma LFP oscillation amplitude and frequency with spiking activity. A. The plot illustrates the relation between the firing rate of each class of neurons and the amplitude of the simultaneously recorded LFP. The circle size shows the percentage of units showing a significant correlation (Spearman correlation; $p<0.05$). The color code displays the average strength of the correlation, as quantified by Spearman's Rho. The plot shows that L6CT activation induces a non-specific and weak correlation between all classes of neurons and LFP amplitude. **B.** Same as panel A for the correlation between firing rate and the frequency of the simultaneously recorded LFP. The plot shows a selective strong correlation between VPm firing rate and LFP frequency across all light intensities, and a high correlation with L23 Fs neurons at low light intensities.

REFERENCES

1. Kirchgessner, M. A., Franklin, A. D. & Callaway, E. M. Context-dependent and dynamic functional influence of corticothalamic pathways to first- and higher-order visual thalamus. *Proc. Natl. Acad. Sci. U. S. A.* **117**, 13066–13077 (2020).
2. Kirchgessner, M. A., Franklin, A. D. & Callaway, E. M. Distinct 'driving' versus 'modulatory' influences of different visual corticothalamic pathways. *Curr. Biol. CB* **31**, 5121-5137.e7 (2021).
3. Kim, J., Matney, C. J., Blankenship, A., Hestrin, S. & Brown, S. P. Layer 6 corticothalamic neurons activate a cortical output layer, layer 5a. *J. Neurosci. Off. J. Soc. Neurosci.* **34**, 9656–9664 (2014).
4. Bortone, D. S., Olsen, S. R. & Scanziani, M. Translaminar inhibitory cells recruited by layer 6 corticothalamic neurons suppress visual cortex. *Neuron* **82**, 474–485 (2014).
5. Ray, S., Crone, N. E., Niebur, E., Franaszczuk, P. J. & Hsiao, S. S. Neural correlates of high-gamma oscillations (60-200 Hz) in macaque local field potentials and their potential implications in electrocorticography. *J. Neurosci. Off. J. Soc. Neurosci.* **28**, 11526–11536 (2008).
6. Nevalainen, P. *et al.* Association of fast ripples on intracranial EEG and outcomes after epilepsy surgery. *Neurology* **95**, e2235–e2245 (2020).
7. Crandall, S. R., Cruikshank, S. J. & Connors, B. W. A corticothalamic switch: controlling the thalamus with dynamic synapses. *Neuron* **86**, 768–782 (2015).
8. Guo, W., Clause, A. R., Barth-Maron, A. & Polley, D. B. A Corticothalamic Circuit for Dynamic Switching between Feature Detection and Discrimination. *Neuron* **95**, 180-194.e5 (2017).

9. Sherman, S. M. & Guillery, R. W. Functional organization of thalamocortical relays. *J. Neurophysiol.* **76**, 1367–1395 (1996).
10. McAfee, S. S., Liu, Y., Dhamala, M. & Heck, D. H. Thalamocortical Communication in the Awake Mouse Visual System Involves Phase Synchronization and Rhythmic Spike Synchrony at High Gamma Frequencies. *Front. Neurosci.* **12**, 837 (2018).
11. Saleem, A. B. *et al.* Subcortical Source and Modulation of the Narrowband Gamma Oscillation in Mouse Visual Cortex. *Neuron* **93**, 315–322 (2017).
12. Hu, H., Hostetler, R. E. & Agmon, A. Ultrafast (400 Hz) network oscillations induced in mouse barrel cortex by optogenetic activation of thalamocortical axons. *eLife* **12**, e82412 (2023).
13. Adesnik, H. & Scanziani, M. Lateral competition for cortical space by layer-specific horizontal circuits. *Nature* **464**, 1155–1160 (2010).
14. Cardin, J. A. *et al.* Driving fast-spiking cells induces gamma rhythm and controls sensory responses. *Nature* **459**, 663–667 (2009).
15. Sohal, V. S., Zhang, F., Yizhar, O. & Deisseroth, K. Parvalbumin neurons and gamma rhythms enhance cortical circuit performance. *Nature* **459**, 698–702 (2009).
16. McNally, J. M. *et al.* Optogenetic manipulation of an ascending arousal system tunes cortical broadband gamma power and reveals functional deficits relevant to schizophrenia. *Mol. Psychiatry* **26**, 3461–3475 (2021).
17. Lu, Y. *et al.* Optogenetically induced spatiotemporal gamma oscillations and neuronal spiking activity in primate motor cortex. *J. Neurophysiol.* **113**, 3574–3587 (2015).

18. Butler, J. L., Mendonça, P. R. F., Robinson, H. P. C. & Paulsen, O. Intrinsic Cornu Ammonis Area 1 Theta-Nested Gamma Oscillations Induced by Optogenetic Theta Frequency Stimulation. *J. Neurosci. Off. J. Soc. Neurosci.* **36**, 4155–4169 (2016).
19. Ray, S., Niebur, E., Hsiao, S. S., Sinai, A. & Crone, N. E. High-frequency gamma activity (80–150 Hz) is increased in human cortex during selective attention. *Clin. Neurophysiol.* **119**, 116–133 (2008).
20. Kucewicz, M. T. *et al.* Dissecting gamma frequency activity during human memory processing. *Brain J. Neurol.* **140**, 1337–1350 (2017).
21. Herrmann, C. S., Munk, M. H. J. & Engel, A. K. Cognitive functions of gamma-band activity: memory match and utilization. *Trends Cogn. Sci.* **8**, 347–355 (2004).
22. Canolty, R. T. *et al.* High gamma power is phase-locked to theta oscillations in human neocortex. *Science* **313**, 1626–1628 (2006).
23. Gaona, C. M. *et al.* Nonuniform High-Gamma (60–500 Hz) Power Changes Dissociate Cognitive Task and Anatomy in Human Cortex. *J. Neurosci.* **31**, 2091–2100 (2011).
24. Mably, A. J. & Colgin, L. L. Gamma oscillations in cognitive disorders. *Curr. Opin. Neurobiol.* **52**, 182–187 (2018).
25. McNally, J. M. & McCarley, R. W. Gamma band oscillations: a key to understanding schizophrenia symptoms and neural circuit abnormalities. *Curr. Opin. Psychiatry* **29**, 202–210 (2016).
26. Shin, Y.-W., O'Donnell, B. F., Youn, S. & Kwon, J. S. Gamma oscillation in schizophrenia. *Psychiatry Investig.* **8**, 288–296 (2011).
27. Gao, R., Peterson, E. J. & Voytek, B. Inferring synaptic excitation/inhibition balance from field potentials. *NeuroImage* **158**, 70–78 (2017).

28. Tatti, R., Haley, M. S., Swanson, O. K., Tselha, T. & Maffei, A. Neurophysiology and Regulation of the Balance Between Excitation and Inhibition in Neocortical Circuits. *Biol. Psychiatry* **81**, 821–831 (2017).
29. Dimwamwa, E. D., Pala, A., Chundru, V., Wright, N. C. & Stanley, G. B. Dynamic corticothalamic modulation of the somatosensory thalamocortical circuit during wakefulness. *Nat. Commun.* **15**, 3529 (2024).
30. Pulvermüller, F., Birbaumer, N., Lutzenberger, W. & Mohr, B. High-frequency brain activity: its possible role in attention, perception and language processing. *Prog. Neurobiol.* **52**, 427–445 (1997).
31. Alvarado-Rojas, C. *et al.* Slow modulations of high-frequency activity (40-140-Hz) discriminate preictal changes in human focal epilepsy. *Sci. Rep.* **4**, 4545 (2014).
32. Fisher, R. S., Webber, W. R., Lesser, R. P., Arroyo, S. & Uematsu, S. High-frequency EEG activity at the start of seizures. *J. Clin. Neurophysiol. Off. Publ. Am. Electroencephalogr. Soc.* **9**, 441–448 (1992).
33. Shahabi, H., Nair, D. R. & Leahy, R. M. Multilayer brain networks can identify the epileptogenic zone and seizure dynamics. *eLife* **12**, e68531 (2023).
34. Wiest, C. *et al.* Finely-tuned gamma oscillations: Spectral characteristics and links to dyskinesia. *Exp. Neurol.* **351**, 113999 (2022).
35. Dubey, A. & Ray, S. Comparison of tuning properties of gamma and high-gamma power in local field potential (LFP) versus electrocorticogram (ECoG) in visual cortex. *Sci. Rep.* **10**, 5422 (2020).
36. Meneghetti, N. *et al.* Narrow and Broad γ Bands Process Complementary Visual Information in Mouse Primary Visual Cortex. *eNeuro* **8**, ENEURO.0106-21.2021 (2021).

37. Olsen, S. R., Bortone, D. S., Adesnik, H. & Scanziani, M. Gain control by layer six in cortical circuits of vision. *Nature* **483**, 47–52 (2012).

38. Cruikshank, S. J., Urabe, H., Nurmikko, A. V. & Connors, B. W. Pathway-specific feedforward circuits between thalamus and neocortex revealed by selective optical stimulation of axons. *Neuron* **65**, 230–245 (2010).

39. Borden, P. Y. *et al*. Thalamic bursting and the role of timing and synchrony in thalamocortical signaling in the awake mouse. *Neuron* **110**, 2836-2853.e8 (2022).

40. Russo, S. *et al*. Thalamic feedback shapes brain responses evoked by cortical stimulation in mice and humans. 2024.01.31.578243 Preprint at https://doi.org/10.1101/2024.01.31.578243 (2024).

41. Halassa, M. M. *et al*. Selective optical drive of thalamic reticular nucleus generates thalamic bursts and cortical spindles. *Nat. Neurosci.* **14**, 1118–1120 (2011).

42. Shu, Y., Hasenstaub, A. & McCormick, D. A. Turning on and off recurrent balanced cortical activity. *Nature* **423**, 288–293 (2003).

43. Jurgens, C. W. D., Bell, K. A., McQuiston, A. R. & Guido, W. Optogenetic stimulation of the corticothalamic pathway affects relay cells and GABAergic neurons differently in the mouse visual thalamus. *PloS One* **7**, e45717 (2012).

44. Naskar, S., Qi, J., Pereira, F., Gerfen, C. R. & Lee, S. Cell-type-specific recruitment of GABAergic interneurons in the primary somatosensory cortex by long-range inputs. *Cell Rep.* **34**, 108774 (2021).

45. Sermet, B. S. *et al*. Pathway-, layer- and cell-type-specific thalamic input to mouse barrel cortex. *eLife* **8**, e52665 (2019).

46. Jouhanneau, J.-S., Kremkow, J. & Poulet, J. F. A. Single synaptic inputs drive high-precision action potentials in parvalbumin expressing GABA-ergic cortical neurons in vivo. *Nat. Commun.* **9**, 1540 (2018).

47. Voigts, J., Deister, C. A. & Moore, C. I. Layer 6 ensembles can selectively regulate the behavioral impact and layer-specific representation of sensory deviants. *eLife* **9**, e48957.

48. Augustinaite, S. & Kuhn, B. Complementary Ca2+ Activity of Sensory Activated and Suppressed Layer 6 Corticothalamic Neurons Reflects Behavioral State. *Curr. Biol. CB* **30**, 3945-3960.e5 (2020).

49. Kaiser, J. & Lutzenberger, W. Human gamma-band activity: A window to cognitive processing. *NeuroReport* **16**, 207 (2005).

50. Pauzin, F. P. & Krieger, P. A Corticothalamic Circuit for Refining Tactile Encoding. *Cell Rep.* **23**, 1314–1325 (2018).

51. Syeda, A. *et al.* Facemap: a framework for modeling neural activity based on orofacial tracking. 2022.11.03.515121 Preprint at https://doi.org/10.1101/2022.11.03.515121 (2022).

52. Wright, N. C. *et al.* Rapid Cortical Adaptation and the Role of Thalamic Synchrony during Wakefulness. *J. Neurosci. Off. J. Soc. Neurosci.* **41**, 5421–5439 (2021).

53. Pala, A. & Stanley, G. B. Ipsilateral Stimulus Encoding in Primary and Secondary Somatosensory Cortex of Awake Mice. *J. Neurosci. Off. J. Soc. Neurosci.* **42**, 2701–2715 (2022).

54. Pachitariu, M., Steinmetz, N., Kadir, S., Carandini, M. & D, H. K. Kilosort: realtime spike-sorting for extracellular electrophysiology with hundreds of channels. 061481 Preprint at https://doi.org/10.1101/061481 (2016).

55. Rossant, C. & Harris, K. D. Hardware-accelerated interactive data visualization for neuroscience in Python. *Front. Neuroinformatics* **7**, (2013).

56. Ganmor, E., Katz, Y. & Lampl, I. Intensity-dependent adaptation of cortical and thalamic neurons is controlled by brainstem circuits of the sensory pathway. *Neuron* **66**, 273–286 (2010).

57. Sederberg, A. J., Pala, A., Zheng, H. J. V., He, B. J. & Stanley, G. B. State-aware detection of sensory stimuli in the cortex of the awake mouse. *PLOS Comput. Biol.* **15**, e1006716 (2019).

58. Sofroniew, N. J., Vlasov, Y. A., Hires, S. A., Freeman, J. & Svoboda, K. Neural coding in barrel cortex during whisker-guided locomotion. *eLife* **4**, e12559.

59. Kvitsiani, D. *et al.* Distinct behavioural and network correlates of two interneuron types in prefrontal cortex. *Nature* **498**, 363–366 (2013).

60. Delorme, A. & Makeig, S. EEGLAB: an open source toolbox for analysis of single-trial EEG dynamics including independent component analysis. *J. Neurosci. Methods* **134**, 9–21 (2004).